

# Estimation of Anisotropic Blur for the Restoration of confocal images

Filip Rooms<sup>a</sup>, Wilfried Philips<sup>a</sup> and Patrick Van Oostveldt<sup>b</sup>

<sup>a</sup> Dept. Telecommunication and Information Processing, Ghent university,  
Sint-Pietersnieuwstraat 41, B-9000 Gent, Belgium

<sup>b</sup> Department Molecular Biotechnology, Ghent university, Coupure Links 653, B-9000 Gent,  
Belgium

## ABSTRACT

We present a novel method for joint estimation of the degradation and restoration of photon-limited images. Our method will be demonstrated on confocal microscope images, since confocal microscopy is an important tool in many academic (fundamental biology, ...) and industrial (material science, pharmaceutical industry, ...) applications. However, the observed images are usually degraded, which hinders analysis and interpretation of the images. Degradation in this kind of images is due to two sources: first, we have blurring due to the band-limited nature of the optical system; second, Poisson noise contaminates the observations due to the discrete nature of the photon detection process.

The proposed method iterates noise reduction and blur estimation using the steerable pyramid transform (which is a variant of the wavelet transform) and deconvolution in the signal domain. These steps are applied in two phases, a training phase and a restoration phase. In the first phase, these three steps are iterated until the blur estimation converges. The second phase is the actual restoration phase.

During the iterations the blur estimation serves as a sharpness measure for the restored image, and is used to control the number of iterations. So, our integrated method provides a completely automatic algorithm where no prior information about the image degradation is required. Our integrated technique was compared with other common restoration techniques for these kind of images, and provided the best restoration results, with least artifacts.

**Keywords:** Richardson-Lucy deconvolution, anisotropic blur estimation, bivariate wavelet shrinkage, Poisson noise, Anscombe transform, steerable pyramid

## 1. INTRODUCTION

Images are produced to record and visualize information. The available information is usually degraded by the observation process, which consists of blurring due to a band limited imaging process (like an optical system), as well as a noise process, which can be due to the recording process by some detector (like a PMT (Photo Multiplier Tube) or a CCD). Image degradation is usually modeled as:

$$g(x, y) = N((h * f)(x, y))$$

with  $g(x, y)$  the blurred image,  $f(x, y)$  the unknown ideal image and  $h(x, y)$  the Point Spread Function (PSF). The symbol  $*$  represents the convolution operator, and models the image blur. The function  $N(\cdot)$  represents the noise processes, caused by the quantum nature of the photon detection process.

The goal of image restoration is to recover  $f(x, y)$  as well as possible from a degraded observed image  $g(x, y)$ . When the degradation parameters (in particular the PSF) are known, one has a classical image restoration problem [1]. However, in some cases the degradation parameters are unknown, and one has two choices: estimating the signal of interest and the degradation parameters simultaneously (blind restoration [2]), or estimating the degradation parameters before starting the restoration process [3]. This paper follows the latter approach.

---

Further author information: (Send correspondence to Filip Rooms)

Filip Rooms: E-mail: frooms@telin.UGent.be, Telephone: +32-9-264.34.15

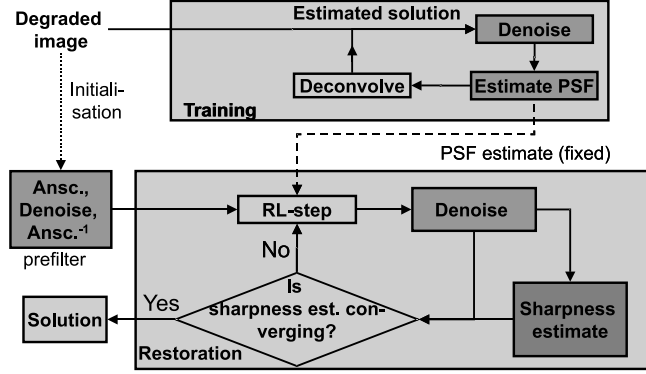


**Figure 1.** The flowchart of the algorithm. Steps in dark gray are executed in the steerable pyramid domain.

In this paper, we present a combined method for degradation estimation and image restoration and that is based on steerable pyramids [4, 5]. To our knowledge, it is the first joint approach for degradation estimation and regularization of deconvolution with steerable pyramids. Only the deconvolution itself isn't calculated with steerable pyramids. In the process some nontrivial problems had to be solved to integrate the different techniques into one framework. Our combined method clearly outperforms normal Richardson-Lucy (RL deconvolution, which is commonly used for restoration of photon-limited images.

The paper is organized as follows: in section 2, our algorithm is discussed, which consists of the following subsections. In subsection 2.1 we give some background on the variant of the wavelet transform, namely the steerable pyramid decomposition and how it is implemented. In subsection 2.2, the noise reduction is discussed, in subsection 2.3, the estimation of the image blur is explained and in subsection 2.4, the deblurring step is explained. In subsection 2.5, a stopping criterium is formulated. In section 3, some experimental results are shown and discussed. Finally, a conclusion is given in section 4.

## 2. OUTLINE OF THE ALGORITHM

The algorithm starts with a steerable pyramid decomposition of the image, followed by noise reduction in the transformed domain. From the noise-reduced subbands, the blur is estimated. After this step, the filtered subbands of the steerable pyramid are recombined. Finally, a Richardson-Lucy deconvolution is applied on the prefiltered image. These different steps are iterated. The estimation of the blur is stable after two iterations, and is used unaltered from then on in each deconvolution step. After this training process, the iterations are restarted with the original degraded image, and the blur estimation is used to control the number of iterations (see fig. 6): when the blur estimation converges, the iterations are stopped.

We will first focus on the steerable pyramid transform, followed by a more detailed explanation of the different steps of the algorithm.

### 2.1. Introduction to steerable pyramids.

In computer vision, one often wants to analyze oriented image structures, like edges under a certain angle. One could filter the image with a range of oriented kernels which cover the whole continuum of angles present in the image. However, this would demand a high computational cost.

In literature, it is shown that one can restrict the computations to filter the image with a fixed set of basic kernels, and interpolate the image filtered with a kernel under an arbitrary direction from the results of the image filtered with the basic kernels [4, 5]. Such a set of kernels is called a steerable filter set. The most illustrative example [5] is a kernel computed as the first partial derivatives in  $x$  and  $y$  of the Gaussian function  $G(x, y) = e^{-(x^2+y^2)} = e^{-r^2}$ .

The partial derivative in  $x$  is given by  $G'_x(x, y) = -2x e^{-r^2}$  and in  $y$  by  $G'_y(x, y) = -2y e^{-r^2}$ . The kernels  $G'_x$  and  $G'_y$  can be interpreted as filters for horizontal and vertical image features respectively. Let  $I(x, y)$  be

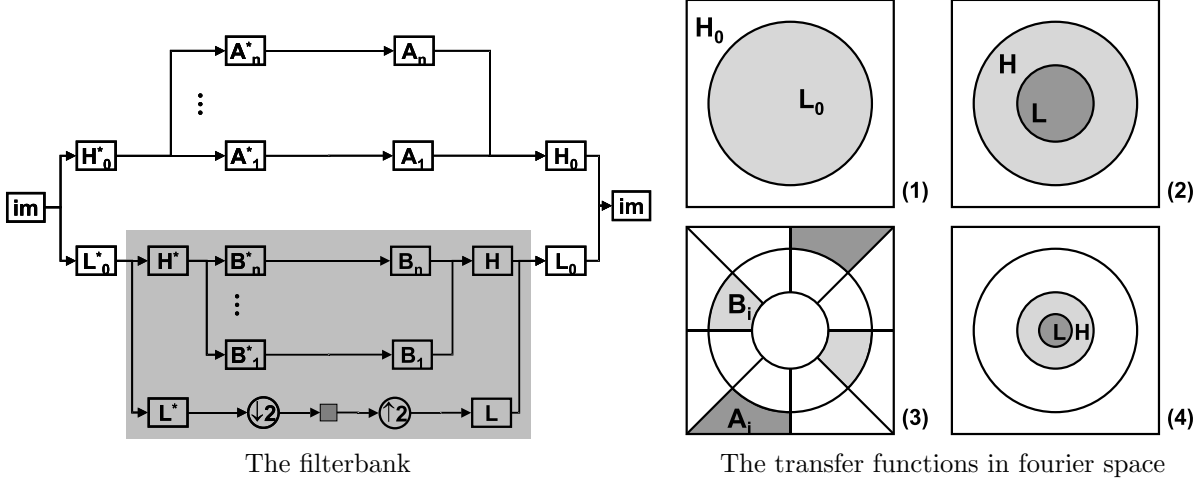


**Figure 2.** The implementation of the pyramid.

the original image and let the symbol  $*$  again be the convolution operator. Then  $R_x(x, y) = (I * G'_x)(x, y)$  is the image filtered for vertical features and  $R_y(x, y) = (I * G'_y)(x, y)$  for horizontal features. These two kernels form a steerable basis set: to compute a kernel  $G'_\theta(x, y)$  to analyze features under an arbitrary angle  $\theta$ , one can take a linear combination of the two basic kernels:

$$G'_\theta(x, y) = \cos(\theta) G'_x(x, y) + \sin(\theta) G'_y(x, y) \quad (1)$$

To calculate  $R_\theta(x, y)$  for a large number of different values of  $\theta$  would be computationally expensive. However, because convolution is a linear operation, it is sufficient to calculate  $R_\theta(x, y)$  as a linear combination of the original image filtered with the two basic kernels:

$$R_\theta(x, y) = \cos(\theta) R_x(x, y) + \sin(\theta) R_y(x, y)$$

which is computationally far less expensive. In [4], the general conditions were given for a set of kernels to form a steerable basis set. In [5], the steerable pyramid is described. This decomposition based on steerable filters is similar to a wavelet decomposition, but has a much better orientation resolution.

To implement the steerable pyramid, we based on the principles in [5] and the practical design on [6]. For this implementation, the image is transformed to the Fourier domain and multiplied with a set of transfer functions in a filterbank structure (see figure 2). Each bandpass is then again transformed into the spatial domain. We start with an initial highpass band  $H_0$  and a lowpass band  $L_0$ . This band  $L_0$  is then subdivided in oriented bandpass fractions  $B_k$  and a residual lowpass band  $L$ . In example 1, only two bandpass fractions were used, which limits the orientation resolution. For the results in this paper, we used 4 oriented subbands per resolution scale.

For the next resolution scale,  $L$  is subsampled and again subdivided in oriented subbands and a lowpass fraction. In figure 2, the part in light grey is recursively applied in the dark square of the bottom subband. A schematic illustration of the transfer functions is given in fig. 2, in which the center of each square corresponds with the DC frequency.

The transfer functions are defined as follows ( $r$  and  $\theta$  are polar coordinates in the Fourier domain):

$$L(r) = \begin{cases} \cos\left(\frac{\pi}{2} \log_2\left(\frac{4r}{\pi}\right)\right) & \frac{\pi}{4} < r < \frac{\pi}{2} \\ 1 & r \leq \frac{\pi}{4} \\ 0 & r \geq \frac{\pi}{2} \end{cases} \quad (2)$$

$$B_k(r, \theta) = H(r)G_k(\theta) \quad k \in [0, K - 1] \quad (3)$$

$$H(r) = \begin{cases} \cos\left(\frac{\pi}{2} \log_2\left(\frac{2r}{\pi}\right)\right) & \frac{\pi}{4} < r < \frac{\pi}{2} \\ 1 & r \geq \frac{\pi}{4} \\ 0 & r \leq \frac{\pi}{2} \end{cases} \quad (4)$$

$$G_k(\theta) = \frac{(K-1)!}{\sqrt{K[2(K-1)]!}} \left[ 2 \cos\left(\theta - \frac{\pi k}{K}\right) \right]^{K-1} \quad (5)$$

For the initial decomposition into  $L_0$  and  $H_0$ , the formulae are given below:

$$L_0(r) = L\left(\frac{r}{2}\right) \quad A_k(r, \theta) = H\left(\frac{r}{2}\right) G_k(\theta) \quad (6)$$

where the  $A_k$ 's form oriented bandpasses of  $H_0$ .

## 2.2. Noise reduction

In photon-limited imaging, the major source of errors is Poisson noise due to the discrete nature of photon detection. Unlike Gaussian noise, Poisson noise is signal dependent, which makes separating signal from noise a very difficult task [7]. However, by applying the Anscombe transform [8], the Poisson data are transformed to data with a Gaussian distribution with unit standard deviation. The Anscombe transform is given by:

$$t(I(x, y)) = 2\sqrt{I(x, y) + \frac{3}{8}}$$

with  $I(x, y)$  data determined by a Poisson process. This transformation allows to use well studied methods for Gaussian noise on data with the much trickier Poisson noise. Then we applied the shrinkage method developed for Gaussian data by Şendur [9], where a bivariate wavelet shrinkage function is proposed:

$$\hat{w}_1(k) = \frac{\left(\sqrt{y_1^2(k) + y_2^2(k)} - \frac{\sqrt{3}\sigma_n^2}{\sigma(k)}\right)_+}{\sqrt{y_1^2(k) + y_2^2(k)}}$$

with  $(x)_+ = \max\{x, 0\}$ .

A denoised coefficient  $\hat{w}_1(k)$  is calculated by using the corresponding noisy coefficient  $y_1(k)$  and its parent  $y_2(k)$ , the coefficient at the same spatial position as  $y_1(k)$ , but in the next coarser resolution scale.  $\sigma_n^2$  denotes the noise variance, and  $\sigma^2(k)$  denotes the marginal variance for the  $k^{\text{th}}$  coefficient (see [9] for details). This algorithm is simple to implement, has a low computational cost and yet provides a state-of-the-art noise reduction performance, and we adapted it for implementation with steerable pyramids. After denoising, the inverse Anscombe transform was applied.

## 2.3. Blur estimation

Our own developed method for blur estimation also operates in the steerable pyramid domain, and is based on estimating the sharpness of the sharpest edges in the image. To analyze edges in the image, we calculate the evolution of the wavelet modulus maxima across scales. Mallat has shown in [10] that this evolution through scales depends on three factors:

- the regularity of the original underlying signal (was it a step edge or a smooth transition?)
- the properties of the wavelet basis functions used in the transform
- the blur of the signal at position  $k$

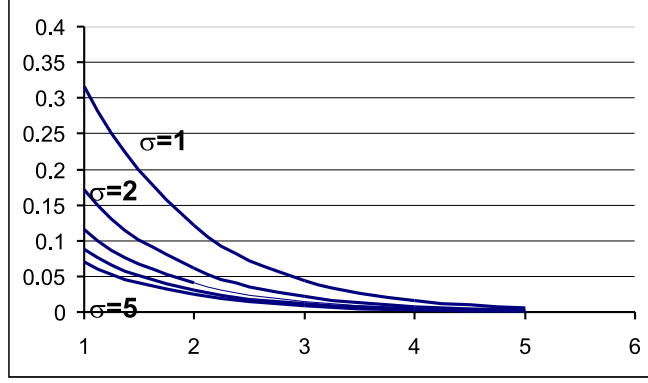


**Figure 3.** Evolution of wavelet coefficients across scales in function of the variance  $\sigma$  of the Gaussian PSF

This means that the blur can be estimated from the evolution of the wavelet coefficients through scales when the other factors are known. For a step edge blurred with a Gaussian PSF with different variances, the evolution of the wavelet coefficients across scales is given for different amounts of blur in figure 2.3.

Practically, we located the modulus maxima of the coefficients of the steerable pyramid in the highest resolution scale and followed the evolution of their magnitude through the different resolution scales. By fitting a curve of the form  $y = a \exp(bx)$  to each of these series of modulus maxima, we obtained a local measure for the blur in the image. Empirically, we saw that the value  $b$  is directly related to the variance of the Gaussian PSF. This was done independently for the four orientations in the pyramid. Assuming that the PSF is Gaussian and spatially independent, we averaged out the blur measures for the different edge pixels for each of the four orientations to obtain a robust estimate for the projection variance of the PSF in the direction perpendicular to the orientation of the subband. This way, we obtain  $\sigma_k$ ,  $k \in [0, K - 1]$ , where  $\sigma_k$  represents the variance projected under  $k\frac{\pi}{4}$ . We know that for a certain  $\sigma_\theta^2$

$$\sigma_\theta^2 = E(\cos(\theta)\mathbf{x} + \sin(\theta)\mathbf{y})^2 \quad (7)$$

$$= \cos^2(\theta)E(\mathbf{x}^2) + \sin^2(\theta)E(\mathbf{y}^2) + 2\cos(\theta)\sin(\theta)E(\mathbf{xy}) \quad (8)$$

$$(9)$$

When  $E(\mathbf{x})$  and  $E(\mathbf{y})$  are zero, we can write:

$$\sigma_\theta^2 = \cos^2(\theta)\sigma_x^2 + \sin^2(\theta)\sigma_y^2 + 2\cos(\theta)\sin(\theta)\sigma_{xy} \quad (10)$$

$$\sigma_{45^\circ}^2 = \frac{1}{2}\sigma_x^2 + \frac{1}{2}\sigma_y^2 + \sigma_{xy} \quad (11)$$

$$\sigma_{135^\circ}^2 = \frac{1}{2}\sigma_x^2 + \frac{1}{2}\sigma_y^2 - \sigma_{xy} \quad (12)$$

$$(13)$$

From these equations, the PSF can be reconstructed using

$$h(X) = \frac{1}{2\pi|\Sigma|^{1/2}} \exp\left(-\frac{1}{2}(X - \mu)^T \Sigma^{-1}(X - \mu)\right) \quad (14)$$

where  $X$  is the vector containing the spatial coordinates,  $\mu = 0$  and

$$\Sigma = \begin{pmatrix} \sigma_x^2 & \sigma_{xy} \\ \sigma_{xy} & \sigma_y^2 \end{pmatrix} \quad (15)$$

This method also works for parametric PSF's other than the Gaussian (e.g., out-of-focus blur, where the PSF is a uniform disc, and the radius has to be estimated).

## 2.4. Deconvolution step

As a deconvolution step, the Richardson-Lucy (RL) algorithm was used. The origin of the so called Expectation Maximization (EM) algorithm was laid by Dempster [11]. It was first applied in image reconstruction by Shepp and Vardi [12]. The algorithm was identical to the algorithms independently obtained by Richardson [13] and Lucy [14]. More background information and references can be found in [15].

Let  $g$  again be the observed, degraded data and  $f$  the ideal image, then the RL algorithm maximizes the likelihood  $P(g|f)$  in case of pure Poisson noise. It has an iterative scheme of the form:

$$\hat{f}_{k+1}(x, y) = \hat{f}_k(x, y) \cdot \left[ \left( h(-x, -y) * \left( \frac{g(x, y)}{h(x, y) * \hat{f}_k(x, y)} \right) \right) (x, y) \right]$$

where  $\hat{f}_{k+1}$  indicates a new estimate of the image,  $g$  represents again the observed, degraded data,  $h$  is the Point Spread Function and  $*$  is the convolution operator. The multiplication and the division are point by point.

This algorithm has following main properties [1]:

- Each estimation  $\hat{f}_k$  is guaranteed to contain only nonnegative pixels
- The sum of the intensities over the whole image is preserved during each iteration
- The log-likelihood of the solution is non-decreasing during the iterations, and converges to a maximum.

## 2.5. Stopping rule and how often to regularize.

In this section, we briefly discuss when to stop the iterations and how often regularization is required. We noticed that the estimation of the blur is decreasing in function of the number of iterations (as expected), as the likelihood of the solution is increasing (illustrated in fig. 6 with an experiment with the confocal image). As an empirical rule, we stop the iterations when the ratio of the blur estimated during previous iteration  $\sigma_{blur, i-1}$  and current iteration  $i$  is converging to 1, i.e., when  $|\frac{\sigma_{blur, i-1}}{\sigma_{blur, i}} - 1| < \epsilon$ , with  $\epsilon$  an empirical threshold chosen to be 0.001.

The calculation of the steerable pyramid is computational intensive, so we would like to minimize the number of transformations to and from the steerable pyramid domain. It is clear that the more often the solution is regularized, the smoother the solution is. In fact, regularizing every iteration may oversmoothen the result, therefore regularizing only every two or three iterations was chosen.

## 3. EXPERIMENTAL RESULTS

We nicknamed our algorithm SPERRiL (**S**teerable **P**yramid-based **E**stimation and **R**egularization of **R**ichardson-Lucy restoration). In fig. 4, we apply SPERRiL on a synthetic image. Here, we show the negatives of the images, to emphasize small intensity fluctuations in the background. Here, fig. 4(a) is the ideal image, fig. 4(b) is a simulated degraded image, where a Gaussian PSF was used, and Poisson noise was applied. In fig. 4(c) the result with classical RL (with Gaussian postblurring) is shown. In fig. 4(d), the result of RL combined with regularization as proposed by Conchello in [16]. Fig. 4(e) is the result of WaRD, a deconvolution approach for with simple wavelet-based regularization [17]. This method doesn't perform optimally here, since it was designed for Gaussian noise. Fig. 4(f) is the result with our own method, Notice also here that noise is better suppressed (less artifacts) with our method than with the other algorithms. For this image, the PSF was available and was used in all algorithms except in SPERRiL, where our own PSF estimation was used. For this experiment, also the ideal image was available, so we could also compare SPERRiL quantitatively with some other methods by calculating the PSNR (expressed in dB), defined by

$$PSNR = 20 \log_{10} (255/RMSE)$$

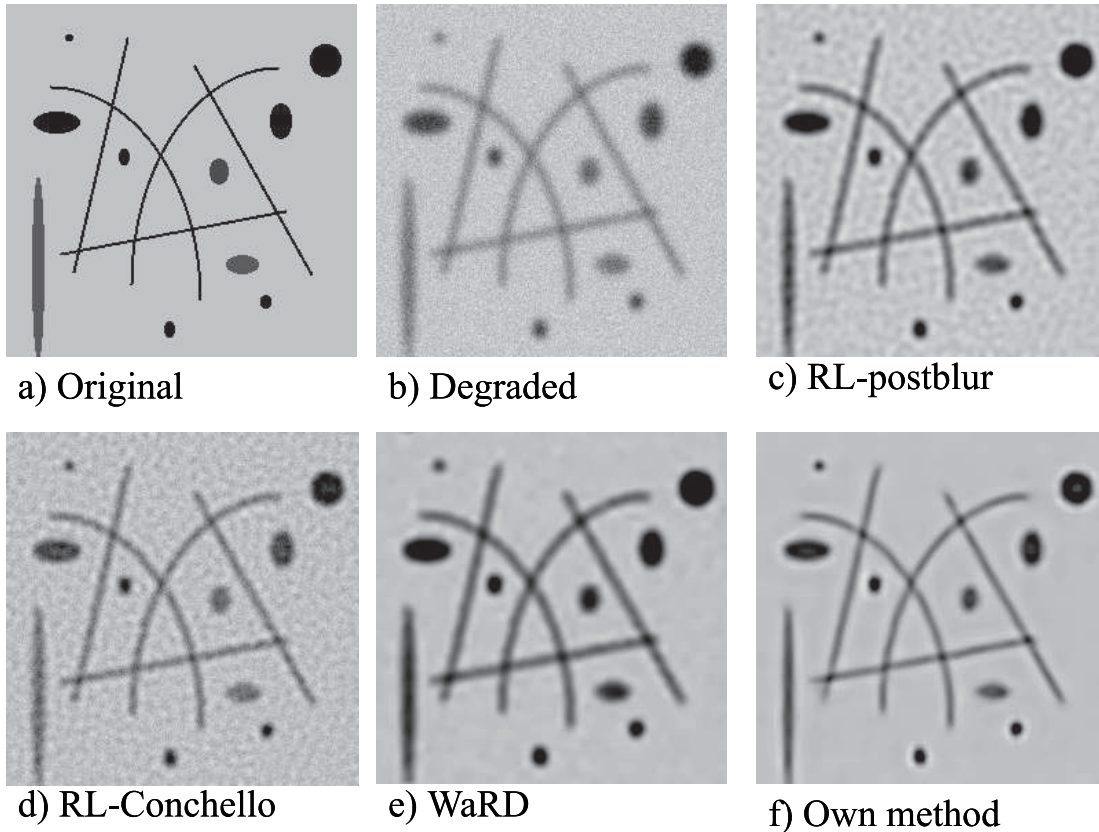


**Figure 4.** Comparison of different methods for restoration of a synthetic image

with

$$RMSE = \sqrt{\sum_i (\hat{f}_i - g)^2}$$

for restoration of this synthetic test image is

image	degraded	Conchello	Gaussian reg.	WaRD	SPERRiL
PSNR	21.62	22.2	22.87	22.7	27.55

In fig. 5, we apply SPERRiL on a real confocal microscope image of a human cell in mitosis, treated with Taxol, a microtubuli stabilizing agent (the dividing nucleus is shown at the lower right). The arc-like structure is the cytoskeleton. Here, fig. 5(a) is the raw image, fig. 5(b) is the result with classical RL (with applying slight gaussian blur after each iteration). In fig. 5(c), the result of RL combined with regularization as proposed by Conchello in [16]. Fig. 5(d) is the result with our own method. Notice also here that noise is better suppressed (less artifacts) with our method than with the other algorithms. For this image, no PSF was available, so a synthetic PSF generated from the first blur estimation was used as input for comparison with the other algorithms. In fig. 6, we plot the image sharpness estimation vs. the number of iterations.

#### 4. CONCLUSIONS AND FUTURE WORK

In this paper, we present an integrated, stable and automatic framework to restore degraded photon-limited images. The estimation of the degradation parameters as well as the regularization of the deconvolution are performed in the steerable pyramid domain. The sharpness estimation is used to formulate a stop criterion for the iterations, thus making the restoration fully automatic.

Future work will also include the deconvolution step in the steerable pyramid domain.

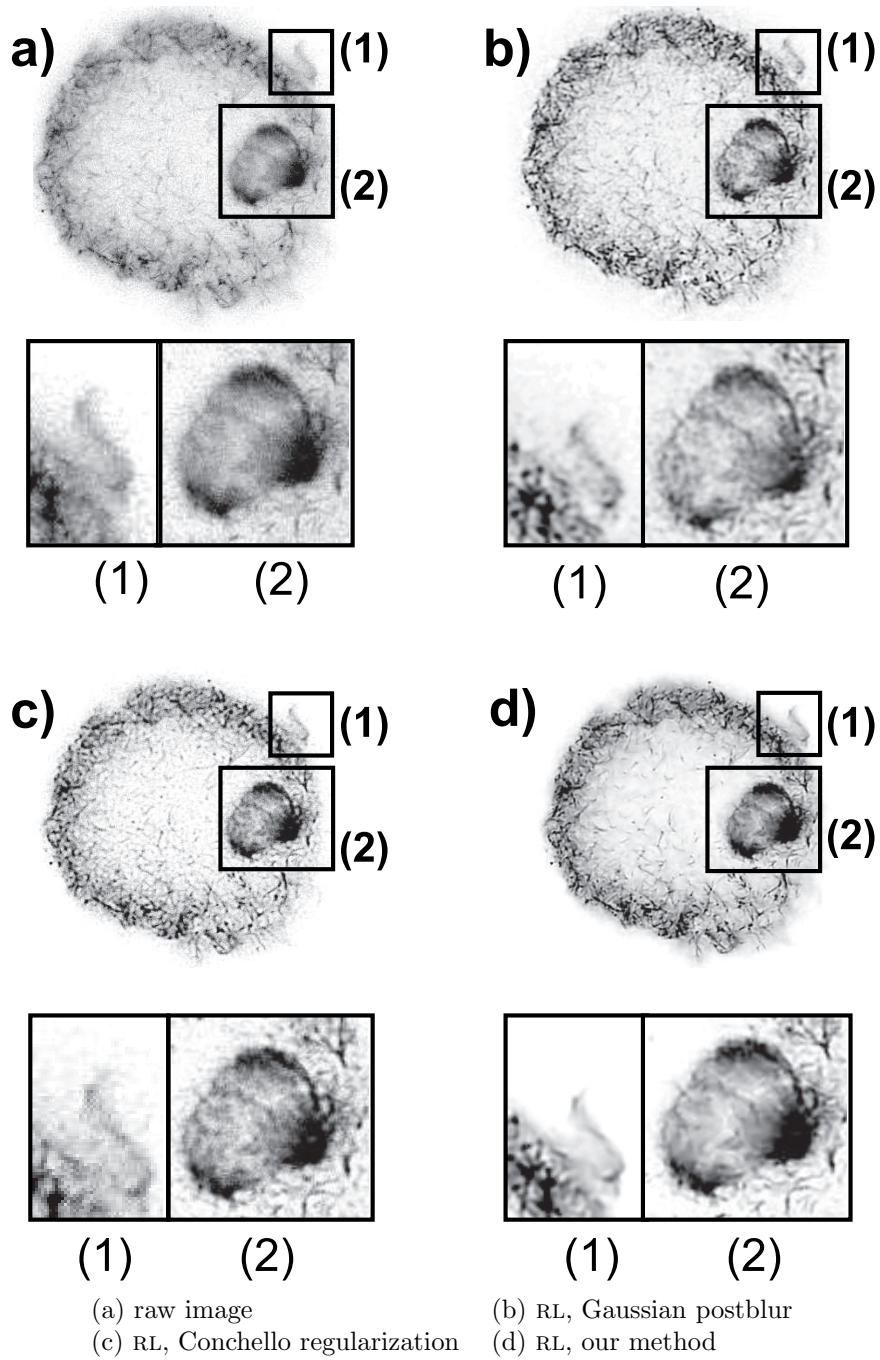


**Figure 5.** Comparison of different methods for restoration of a confocal image

### 5. ACKNOWLEDGEMENTS

This research was financed with specialization scholarship of the Flemish Institute for Stimulation of Scientific-Technical research in the industry (IWT). Image 5 was recorded by prof. dr. P. Van Oostveldt of the Lab. Biochemistry and Molecular Cytology at the Faculty of Agricultural and Applied Biological Sciences of Ghent University.

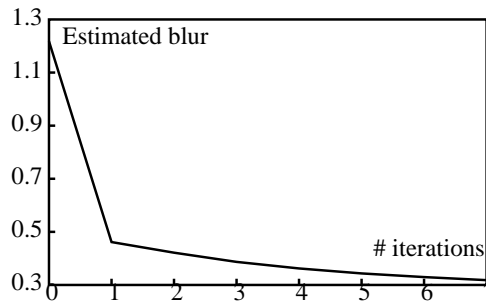


Figure 6. Blur estimation vs. number of iteration

## REFERENCES

1. M. Bertero and P. Boccacci, *Introduction to inverse problems in imaging*, Institute of Physics Publishing, Bristol and Philadelphia, 1998.
2. D. Kundur and D. Hatzinakos, "Blind image deconvolution," *IEEE Signal Processing Magazine* **13**, pp. 43–64, May 1996.
3. A. K. e. Katsaggelos, *Digital Image Restoration*, Springer-Verlag, Berlin, Heidelberg, New York, 1989.
4. W. T. Freeman and E. H. Adelson, "The design and use of steerable filters," *IEEE Trans. Pattern Analysis and Machine Intelligence* **13**(9), pp. 891–906, 1991.
5. E. P. Simoncelli, W. T. Freeman, E. H. Adelson, and D. J. Heeger, "Shiftable multi-scale transforms," *IEEE Trans. Informations Theory* **38**(2), 1992.
6. J. Portilla, V. Strela, M. Wainwright, and E. P. Simoncelli, "Image denoising using gaussian scale mixtures in the wavelet domain," *Technical Report TR2002-831, Computer Science Department, Courant Institute of Mathematical Sciences, New York University (to be published in IEEE Transactions on Image Processing in 2003)*, September 2002.
7. R. D. Nowak and R. G. Baraniuk, "Wavelet-domain filtering for photon imaging systems," *IEEE Trans. Image Processing*, pp. 666–678, May 1999.
8. J.-L. Starck, F. Murtagh, and A. Bijaoui, *Image Processing and Data Analysis, the multiscale approach*, Cambridge University Press, 1998, 2000.
9. L. Şendur and I. W. Selesnick, "Bivariate shrinkage functions for wavelet-based denoising exploiting inter-scale dependency," *IEEE Trans. Signal Processing* **50**, pp. 2744–2756, November 2002.
10. S. Mallat, *A wavelet tour of signal processing (2nd ed.)*, Academic Press, Oval Road, London, 1998, 1999.
11. A. P. Dempster, N. M. Laird, and D. B. Rubin, "Maximum likelihood from incomplete data via the em algorithm," *Journal of the Royal Statistical Society Series B* **39**, pp. 1–38, November.
12. L. A. Shepp and Y. Vardi, "Maximum likelihood reconstruction for emission tomography," *IEEE Trans. Med. Imaging* **1**(2), pp. 113–122, 1982.
13. W. H. Richardson, "Bayesian-based iterative method of image restoration," *Journal of the Optical Society of America* **62**, pp. 55–59, January.
14. L. B. Lucy, "An iterative technique for the rectification of observed distributions," *The Astronomical Journal* **79**, pp. 745–754, June.
15. R. Molina, J. Núñez, F. J. Cortijo, and J. Mateos, "Image restoration in astronomy, a bayesian perspective," *IEEE Signal Processing Magazine*, pp. 11–29, March 2001.
16. J.-A. Conchello and J. G. McNally, "Fast regularization technique for expectation maximization algorithm for optical sectioning microscopy," in *Proceedings of SPIE Three-Dimensional Microscopy: Image Acquisition and Processing III, San Jose*,
17. R. Neelamani, H. Choi, and R. G. Baraniuk, "Wavelet-domain regularized deconvolution for ill-conditioned systems," in *IEEE International Conference on Image Processing - ICIP-1999, vol. 1, pgs. 204–208 Kobe, Japan, 2002*.